

Project 1:

Effective Field Theory Modeling

Jonatan Haraldsson
jonhara@chalmers.se

Oscar Stommendal
oscarsto@chalmers.se

Abstract

Parameter estimation with Bayesian inference of a simple model based on Chiral Effective Field Theory for nuclear interactions was realized in a `Python` environment. Figures with Markov Chain Monte Carlo (MCMC) sampled posterior distributions of estimated parameter values and observables, in this case binding energies of ${}^3\text{H}$, ${}^4\text{He}$, the radius $r({}^4\text{He})$ and the beta-decay half-life $fT_{1/2}$ of ${}^3\text{H}$, was created and compared to a more advanced set-up used by Wesolowski *et al.* [1]. Due to simplifications in the used model, a slight shift in the posterior of $r({}^4\text{He})$ was observed, which could have led to a less accurate parameter estimation. Unlike Wesolowski *et al.*, the model discrepancy, i.e. errors related to the model, was fixed in this analysis, which gave normally distributed parameters and observables. As an extra task, one of the terms in the model discrepancy was set as a hyperparameter, which gave t -distributed parameters. The predictive distributions for the observables showed alternating behavior regarding distribution type, which was concluded to depend on the sampling setup.

October 2024

Course: *Learning from Data, 7,5 hp*

Course Code: *TIF285*

Physics, MSc.

CHALMERS UNIVERSITY OF TECHNOLOGY



CHALMERS
UNIVERSITY OF TECHNOLOGY

1 Introduction

Scientific modeling – relating models with an unknown sets of model parameters to empirical data, is an essential tool to gain deeper understanding, not only in physics, but in vast fields of scientific research. Usually, this is done by comparing the model’s outputs to experimental data, while simultaneously tuning the model parameters to obtain a model with desired accuracy. A well-known and -tested approach is to update model parameters through so called Bayesian inference, a process where probabilities for certain values of model parameters are obtained. Bayesian inference is mostly done numerically and with the increased computational power of today, this approach of scientific modeling has successfully provided insight into systems that cannot be described analytically.

In nuclear physics, modeling a system of atomic nuclei is one example of where Bayesian inference can be used to obtain information such as binding energies, nuclear radii and halflives. This was done by Wesolowski *et al.*, where binding energies of ${}^3\text{H}$, ${}^4\text{He}$, the (point-proton) radius (R_p) of ${}^4\text{He}$ and the beta-decay half-life ($fT_{1/2}$) of ${}^3\text{H}$ was estimated [1]. To approximate the atomic interactions described by quantum field theory, the model used by Wesolowski *et al.* was based on an effective field theory (EFT) known as Chiral Effective Field Theory (χ EFT). Since Quantum Chromodynamics (QCD), the fundamental theory of strong interactions within quantum field theory, is not practical for low-energy descriptions due to its complexity, EFT provides a more manageable alternative.

In this report, the aim is to reproduce results from [1] using a simpler, yet, similar model based on EFT. Furthermore, uncertainties, both experimental and theoretical, are discussed with extra focus on the model discrepancy term.

2 Theory

The main goal with modeling is to find a model, M with parameters $\boldsymbol{\theta}$, such that $\mathbf{y}_{\text{exp}} = M(\boldsymbol{\theta}; \vec{x})$, where \mathbf{y}_{exp} are experimental data and \vec{x} are dependent variables. However, due to observational errors ($\delta\mathbf{y}_{\text{exp}}$) and errors related to the model (δM , model discrepancy), a more accurate description would be

$$\mathbf{y}_{\text{exp}} = M(\boldsymbol{\theta}; \vec{x}) + \delta\mathbf{y}_{\text{exp}} + \delta M.$$

With the Bayesian approach, obtaining parameters given information I and model M is done according to Bayes’ Theorem, which for \mathbf{y}_{exp} and $\boldsymbol{\theta}$ is given by

$$\underbrace{p(\boldsymbol{\theta}|\mathbf{y}_{\text{exp}}, M, I)}_{\text{Posterior}} = \frac{\overbrace{p(\mathbf{y}_{\text{exp}}|\boldsymbol{\theta}, M, I)}^{\text{Likelihood}} \overbrace{p(\boldsymbol{\theta}|M, I)}^{\text{Prior}}}{\underbrace{p(\mathbf{y}_{\text{exp}}|M, I)}_{\text{Model evidence}}}. \quad (1)$$

The posterior, i.e. the probability density function of $\boldsymbol{\theta}$ giving \mathbf{y}_{exp} , is commonly the quantity of interest, since it contains information on values of $\boldsymbol{\theta}$. However, obtaining a posterior distribution by only using Equation 1 is often numerically heavy, since it requires an extensive number of calculations to cover the whole parameter space. To combat this, sampling the logarithm of the posterior using a Markov Chain Monte Carlo (MCMC) method provides a similar distribution with less calculations.

Instead of evaluating the posterior at every point, MCMC sampling evaluate the log posterior, $\log [p(\boldsymbol{\theta} | \mathbf{y}_{\text{exp}}, M, I)]$, at a sufficiently large and cleverly chosen set of parameter values with the goal of obtaining an identical distribution. After each evaluation, the value is passed through an acceptance function, that either accepts or rejects the sample. Subsequently, new parameter values are proposed independently according to a proposal distribution and the new posterior value is passed through the acceptance function once again.

To ensure the model converges to the correct distribution, a sufficiently large number of iterations is required. Furthermore, the procedure is often initialized from several different starting points simultaneously and then run in parallel chains. Each run chain is commonly referred to as a *walker*. To check convergence and spot unwanted correlations during the sampling process, the sampled values of each walker can be plotted as a function of iterations in a so-called *trace plot*.

The model considered in this project relies upon the two parameters c_D and c_E , which both originate from the EFT description of the strong force. In addition, the model discrepancy, δM , is given by

$$\delta M_i = \sqrt{\frac{y_{\text{exp},i} \bar{c} Q^{k+1}}{1 - Q^2}}, \quad (2)$$

where $y_{\text{exp},i}$ is the experimental value for observable i , Q is a variable emerging from the EFT expansion (a way of breaking a complex system into smaller parts, e.g. by starting with the most important ones) and \bar{c} is a scale parameter used to control the relative correction at each expansion step [1], [2].

3 Method

In the current section, methods used to reproduce the results found by Wesolowski *et al.* [1] are presented, with particular attention to methodological differences, as these play a significant role in the subsequent discussion of the results. Note that the complete Python script used in the project is available on [Github](#).

3.1 Studies of the posterior with individual data likelihood

Initially, a contour plot similar to figure 6 in [1] with constraints on binding energies $E(^3\text{H})$, $E(^4\text{He})$, radius $r(^4\text{He})$ and half-life ($fT_{1/2}$) was constructed using a Bayesian approach. This was done by implementing functions for the log-prior, -likelihood and -posterior. As outlined by [1], the prior for the parameters was set to

$$p(c_D, c_E | I) = \mathcal{N}(c_D; \mu = 0, \sigma = 5) \mathcal{N}(c_E; \mu = 0, \sigma = 5).$$

The likelihood was evaluated individually for each observable, and was given by

$$p(y_{\text{exp},i} | c_D, c_E, \sigma_i, I) = \mathcal{N}(y_{\text{th},i}(c_D, c_E), \sigma_i),$$

where $y_{\text{exp},i}$ is the measured experimental value for each observable presented in Table 1 in [1] and $y_{\text{th},i}(c_D, c_E)$ is the model prediction for each observable.

Following the approach of [1], the error term σ_i was initially set to only contain the combined error from the experiments and the precision of the many-body solver used to calculate the different observable values, i.e. the adopted uncertainties from Table 1 in [1], σ_{adp} was

used. The likelihood was also evaluated with σ_i , containing the error describing the model discrepancy, namely the EFT error presented in Equation 2. In other words, $\sigma_i = \sigma_{adp} + \sigma_{EFT}$. Similar to [1], fixed values of $\bar{c} = 1$ and $Q = 0.33$ were used.

Subsequently, the posterior for each observable, given by the exponential of the log-posterior, was evaluated for both likelihoods (with and without the EFT error term) on a grid ($3\,000 \times 3\,000$ points) with $c_D \in [-2.5, 2.5]$, $c_E \in [-1, 1]$. The different posterior distributions were then plotted as contour plots, with constraints capturing 39 % of the posterior density mass, which is consistent with the method used in [1].

3.2 Posterior sampling

After studying the posteriors of individual likelihoods, code was implemented to sample from the posterior distributions. However, this time the likelihood was combined from two sets of observables, where set 1 consisted of $\{E(^4\text{He}), r(^4\text{He})\}$ and set 2 of $\{E(^3\text{H}), E(^4\text{He}), r(^4\text{He}), fT_{1/2}\}$. Using the latter set resulted in a plot similar to figure 3 in [1]. The sampling was performed using the Python package `emcee` – a free implementation of Markov Chain Monte Carlo sampling, as outlined by [1].

Following [1], only the second case of the error term σ_i in the likelihoods, i.e. the case with the EFT error, was considered. In contrast to Wesolowski *et. al* [1], who included the error parameters \bar{c} and Q in the sampling, the values of \bar{c} and Q was kept fixed as before. For further comments and discussion on this topic, see Section 3.4.

During the sampling, traces were plotted for different starting vectors for c_D and c_E to visualize the convergence of the sampler. This gave an indication of how many initial iterations to discard and gave a hint towards valid initial guesses for c_D and c_E . In conclusion, it was decided to discard 500 sampler iterations and draw initial guesses from the normal distribution $\mathcal{N}(\mu = 0, \sigma = 1)$. A collection of final trace plots are given in Appendix A.

Lastly, the `emcee` sampler was executed for both sets of observables with 50 500 iterations (including discarded ones), producing a total of 1 250 000 samples using 25 walkers. In contrast, [1] run 52 000 iterations (including 2 000 discarded) with 50 walkers. After sampling, the result was plotted in a corner plot using the package `corner`, visualizing the distributions for the c_D and c_E samples.

To verify the distribution type of the samples, the number of degrees of freedom (ν) for fitted t_ν -distributions were counted. Since both distributions clearly were Gaussian, the sample distributions were fitted to a multivariate normal distribution for both sets of observables using the `scipy` library. This was used to

- (i) Plot marginalized, fitted PDFs for the histograms of c_D and c_E ,
- (ii) Visualize the 1- and 2σ intervals in the joint posterior contour plots for both sets of observables by evaluating the fitted distribution over a grid.

3.3 Posterior predictive distributions

Subsequently, the function `fewnucleonEmulator` was employed together with the samples of c_D and c_E to generate predictive distributions for the different observables, which were again visualized using `corner`. This resulted in a corner plot similar to Figure 4 in [1]. As before, these predictive distributions were fitted to a multivariate t_ν distribution using `scipy` and ν was counted. Similarly, this was done to plot marginalized, fitted PDFs for the histograms of each observable and to visualize the 1 - and 2σ intervals in the contour plots by marginalizing over every pair of observables.

3.4 Extra: Sample the error model

As an extra task, the figures concerning the set of four observables from Section 3.2 and 3.3 were reproduced with the addition of also sampling the error parameter Q . In contrast, Wesolowski *et al.* introduced both parameters \bar{c} and Q in the sampling. Following [1], Q is assigned a Beta distribution prior with $\alpha = 3$ and $\beta = 5$, which gave the prior

$$p(c_D, c_E, Q|I) = \mathcal{N}(c_D; \mu = 0, \sigma = 5) \mathcal{N}(c_E; \mu = 0, \sigma = 5) \mathcal{B}(Q; \alpha = 3, \beta = 5).$$

With the addition of sampling Q , the likelihood is now given by

$$p(y_{exp,i}|c_D, c_E, Q, \sigma_i, I) = \mathcal{N}(y_{th,i}(c_D, c_E), \sigma_i(Q)),$$

where Q enters the model by determining the value of each σ_i . Note that the value of \bar{c} in the EFT error was still kept fixed at $\bar{c} = 1$.

After the log prior, -likelihood and -posterior functions were implemented, the log-posterior was sampled with `emcee` using 50 walkers and 52 000 iterations (of which 2 000 were discarded) as done in [1]. Trace plots were again used primarily to give valid initial guesses for c_D - and c_E walkers. For Q , the initial walker vector was drawn from a Beta distribution with $\alpha = 3$ and $\beta = 5$, consistent with its prior.

After sampling, the marginalized sample distributions for c_D and c_E were plotted using `corner` (Q was marginalized). The samples were then fitted to a multivariate t -distribution, as done by [1]. However, as Wesolowski *et. al* did not mention how this was done, an own approach of fitting, described in appendix B, was implemented. For the predictive distributions, `fewnucleonEmulator` was once again used for each of the four observables with the samples for c_D and c_E . The predictive distributions were then plotted using `corner`.

4 Results and discussion

In this section, the results together with short comments and interpretations connected to the results found by Wesolowski *et al.* [1] are presented.

4.1 Studies of the posterior with individual data likelihood

Figures 1a and 1b, constructed in a similar way as figure 6 in [1], show constraints on the model parameters c_D and c_E , with individual data likelihood evaluations with and without the EFT error. Compared to the result in [1], the MAP point (maximum a posteriori, i.e. the point (c_D, c_E) with the highest posterior value) differ slightly, however, this is expected due to some differences in the model used in this project along with other approximations.

In addition, if Figures 1a and 1b are compared to the corresponding figures in [1], the constraints concerning $r(^4\text{He})$, i.e. the posterior PDF, deviate more from the ones of $E(^4\text{He})$ and $E(^3\text{H})$. Due this shift in the posterior PDF of $r(^4\text{He})$, one cannot find an optimal pair of parameters (c_D^*, c_E^*) within the 39 % highest posterior density region for every observable. In [1], however, such pairs could be found in the case with EFT error included. In conclusion, this emphasizes some of the limitations with the model used.

Figure 1 also suggests a positive correlation of observables $E(^4\text{He})$, $E(^3\text{H})$ and $r(^4\text{He})$, i.e. their dependence of parameters c_D and c_E are essentially the same. This also clarifies the use of $fT_{1/2}$, since this puts strong constrains on the grid of (c_D, c_E) compared to the remaining observables. With the goal of estimating the parameters validly, it is thus important to include $fT_{1/2}$ when performing the estimation. Likewise, if $r(^4\text{He})$, due to its shift, were to be excluded as an observable, the method should be able to give a more accurate (c_D^*, c_E^*) .

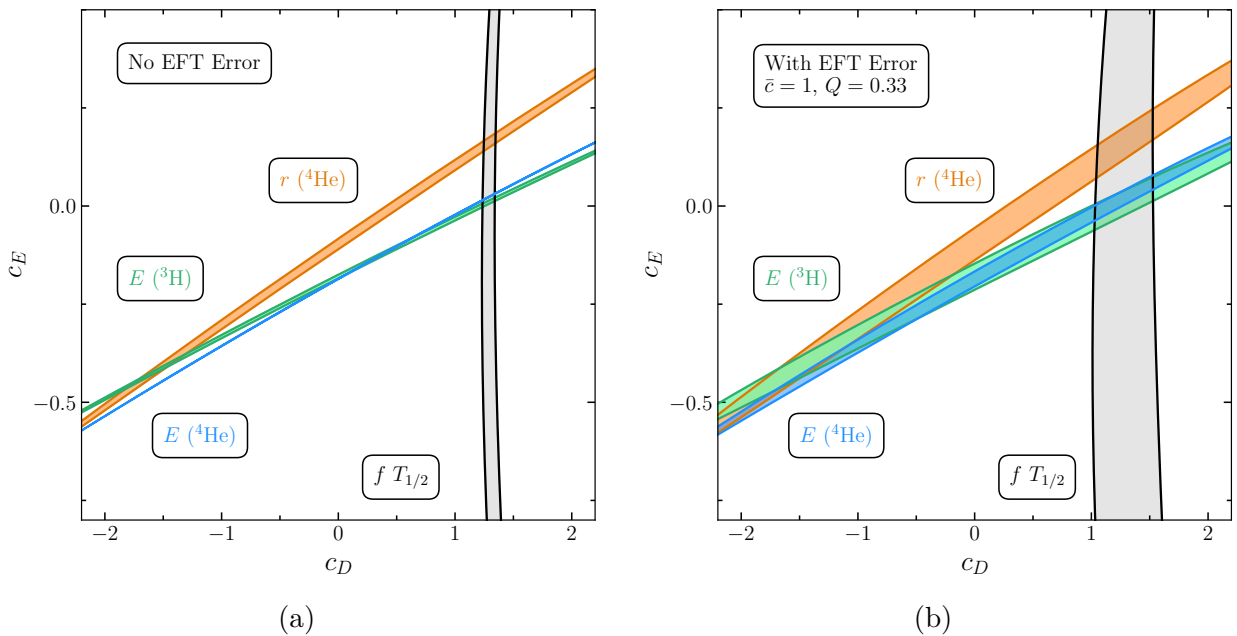


Figure 1: Constraints on c_D and c_E from individual data likelihood evaluations both with (a) and without (b) the EFT truncation error term. Filled regions denote 39 % probability density mass of the posterior distributions for the four observables $E(^3\text{H})$, $E(^4\text{He})$, $r(^4\text{He})$ and $fT_{1/2}$. This corresponds to 1σ intervals for a 2D Gaussian distribution. Note in particular that the MAP point has changed compared to the results presented by Wesolowski *et.al.*, together with the posterior PDFs as a function of the parameters [1].

4.2 Posterior sampling

Figure 2 contains corner plots from two MCMC sample runs of c_D and c_E with the combined likelihood of observables $\{E(^4\text{He}), r(^4\text{He})\}$ (a) and $\{E(^3\text{H}), E(^4\text{He}), r(^4\text{He}), fT_{1/2}\}$ (b). From Table 1, which contains the number of degrees of freedom for the test-fitted t -distributions, it can be concluded that the samples are normally distributed in all cases. When comparing samples for the two parameters, c_D tends to have higher deviation in both runs. Furthermore, the run with four observables tends give less deviation in both c_D and c_E . By the shape of the multivariate distribution, especially in Figure 2a, there is a positive correlation between the two parameters, as also found by [1].

The higher deviation and stronger correlation in set 1 could be understood by considering the posteriors of $E(^4\text{He})$, $r(^4\text{He})$ in Figure 1b. In that figure, the posteriors are indeed positively correlated and have a wide overlapping region of possible parameter values, especially in c_D . When all parameters are included, as in set 2, $fT_{1/2}$ limits the overlapping region, and thus reducing deviations in c_D and c_E .

Comparing Figure 2b to Figure 3 in [1], the two plots show distributions of c_D and c_E with similar deviations but slightly altered modes. In addition, the modes in figure 2a ($c_D \approx -1.6$, $c_E \approx -0.5$) aligns well with the overlapping regions in figure 1b.

Table 1: Number of degrees of freedom for fitted t_ν -distributions for the two cases. For both sets, ν is considered large.

Set of parameters	Parameter	Degrees of freedom ν
Set 1: two observables	c_D	27
Set 1: two observables	c_E	$8,3 \times 10^9$
Set 2: four observables	c_D	$5,1 \times 10^2$
Set 2: four observables	c_E	$7,1 \times 10^8$

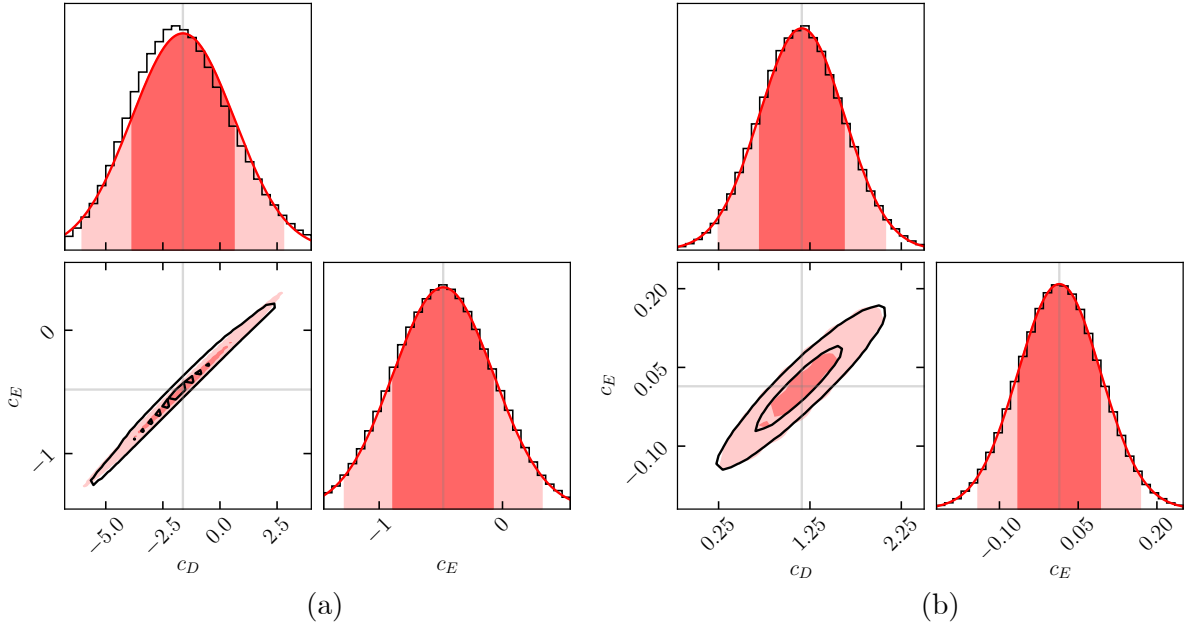


Figure 2: The posterior PDF as a function of c_D and c_E using the combined likelihood of $\{E(^4\text{He}), r(^4\text{He})\}$ (a) and $\{E(^3\text{H}), E(^4\text{He}), r(^4\text{He}), fT_{1/2}\}$ (b). The black histograms and contour lines correspond to the pure MCMC samples of the parameters, while the red curves and ellipses are results of a multivariate fit of the samples. The filled regions represents 1- and 2 σ intervals, which contains 68 % and 95 % of the probability mass in the 1D case, and 39 % and 86 % in the 2D case. The black contour lines corresponds to 39 % and 86 % in the unfitted distribution. Dimmed gray lines correspond to the means of the fitted sample (marginalized) distributions.

4.3 Posterior predictive distributions

A corner plot of the predictive distributions the posterior of four observables are given in Figure 3. The joint distributions of $E(^4\text{He})$, $E(^3\text{H})$ and $r(^4\text{He})$ indicate a slight positive correlation between the observables, which is also confirmed by the positive correlation in Figure 1b/1a. For $fT_{1/2}$, on the other hand, there seems to be a slight negative correlation to $r(^4\text{He})$, and no significant correlations to the binding energies. From a physics perspective, a positive correlation between observables, such as seen between $E(^3\text{H})$ and $E(^4\text{He})$, indicates that if a set of parameters increase $E(^3\text{H})$ this set will also increase $E(^4\text{He})$. It is reasonable, in this particular case, since these observables contain the same basic quantity (binding energy) and probably are computed similarly.

Although the resulting distributions were obtained with fixed error parameters, similar correlations are also found by Wesolowski *et.al.* in [1]. Moreover, the observable distributions are, as the parameter-counterparts normally distributed. This is, as explained in section 3.2, reasonable when using fixed values of \bar{c} and Q . Also note that the predictive distribution of $r(^4\text{He})$ completely misses the experimental value, which also can be seen in Figures 1a and 1b. This is, as then, due to the simplified model used in this project.

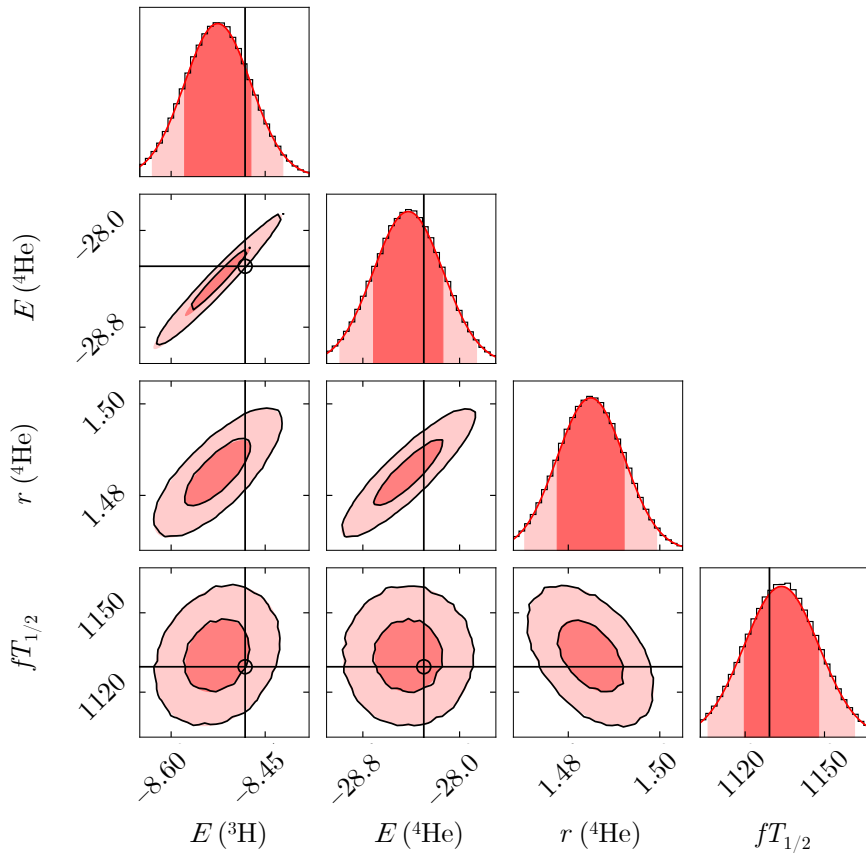


Figure 3: Prediction distributions from the sampling of the posterior for all observables. Black histograms and contour lines are results of the MCMC sampling, while red lines and ellipses result from a multivariate normal distribution fit. Filled regions denote 1- and 2 σ intervals, which contains 68 % and 95 % in the 1D cases, and 39 % and 86 % in the 2D cases. The black contours correspond to 39% and 86% of the unfitted distribution. The black lines and circles represent the experimental data of the observables as presented in [1].

4.4 Extra task: Sample the error model

In Figures 4 and 5, samples of parameters c_D and c_E and predictive distributions for the observables with Q as a model parameter are given. In contrast to figure 2a and 3, the distributions for c_D and c_E now have the characteristic heavier tails of a t -distribution. As explained by [1], this is reasonable since we now also sample with Q , which results in t -distributed samples. The best fit for the multivariate t -distribution was in the case of c_D and c_E samples found with $\nu = 2.5$ degrees of freedom, and a scale matrix of

$$S = \begin{bmatrix} 0.200 & 0.030 \\ 0.030 & 0.006 \end{bmatrix}.$$

Although we presumably used both a different model and a different method of fitting these values, they are close to what was found by Wesolowski *et. al* [1]. In addition, a more similar result are obtained in this case compared to the samples without Q as a model parameter.

An additional comment about the model parameter Q can be done when examining Figure 4 in Appendix C. From this, Q show no correlation with the parameters c_D and c_E . Furthermore, the sampled posterior for Q are similarly shaped as its Beta-distributed prior. This is somewhat expected since Q only enters the model in the EFT error term, and does not directly influence the other model parameters.

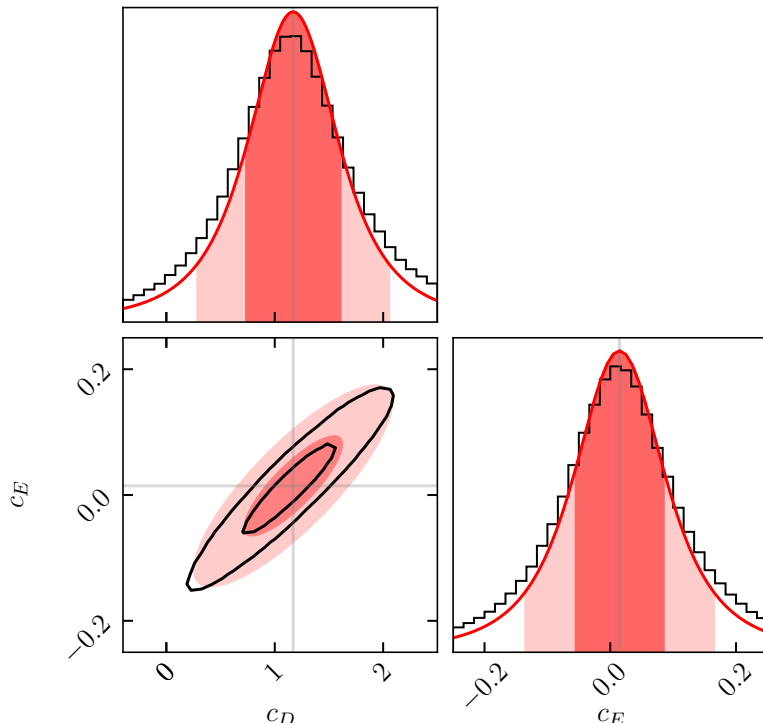


Figure 4: The posterior PDF as a function of c_D and c_E after sampling with the error parameter Q . The black histograms and contour lines correspond to the pure MCMC samples of the parameters. The red curves and ellipses are results of a multivariate t -distribution fit of the samples. The filled regions represents 1- and 2σ intervals, which contains 59 % and 84 % of the probability mass in the 1D case, and 30 % and 72 % in the 2D case. The black contour lines corresponds to 30 % and 72 % in the unfitted distribution. Dimmed gray lines correspond to the means of the fitted sample (marginalized) distributions.

In Figure 5, the predictive distributions of all observables are showed. Here, only the predictive distribution of $E(^3\text{H})$ showed signs of a normal distribution (i.e., a large ν when trying to fit it to a t -distribution). The fit described by the red color was made as described in Appendix B, with the only change that the value of ν was set to 2.5, which was found optimal when fitting the samples of c_D and c_E . After several tries to only obtain t -distributed observables, it can be concluded that the number of walkers/iterations made are important, and due to the lack of computational power, runs with a sufficient number of walkers/iterations to obtain t -distributed samples of $E(^3\text{H})$ was not conducted. Lastly, also sampling \bar{c} , as done in [1], would probably have emphasized the t -distributive samples even more.

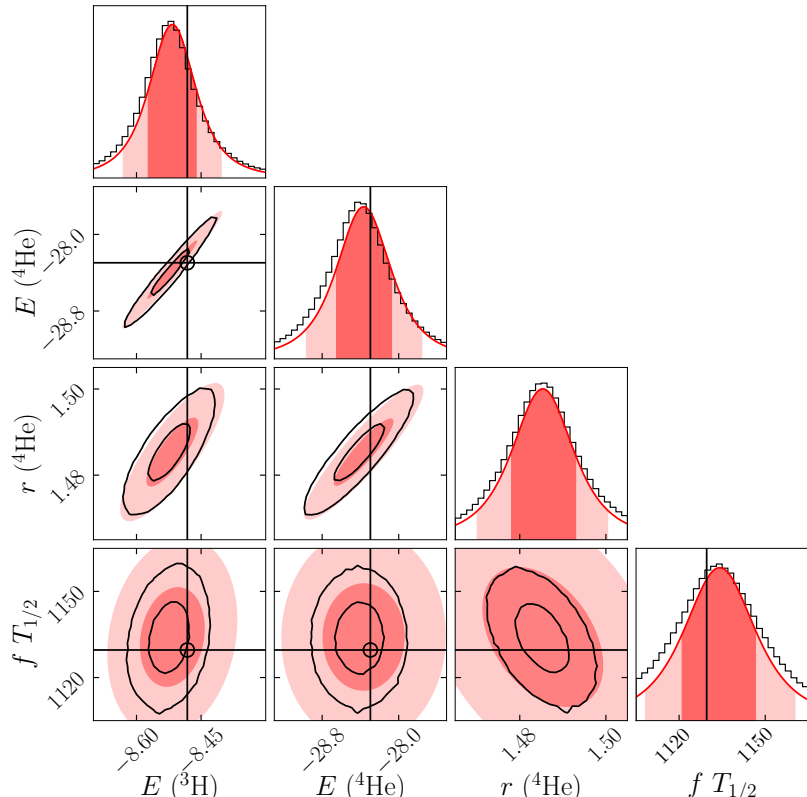


Figure 5: Prediction distributions from the sampling of the posterior for all observables when including the error term Q . Black histograms and contour lines are results of the MCMC sampling, while red lines and ellipses result from a multivariate t -distribution fit. Filled regions result from the fit and denote 1- and 2 σ intervals, which contains 59 % and 84 % in the 1D cases, and 30 % and 72 % in the 2D cases. The black contours correspond to 39 % and 86 % of the unfitted distribution. The black lines and circles represent the experimental data of the observables as presented in [1].

5 Conclusion

By MCMC sampling posteriors for parameters in a simple model for atomic observables based on the Chiral Effective Field Theory, similar results as in [1] were obtained. Since a small shift is observed in the posterior of $r(^4\text{He})$, the observables do not overlap in the parameter space and there are consequently no set of parameters that can describe all observables optimally. When the model discrepancy terms (\bar{c} and Q) are fixed, the sampled observables and parameters follow a Gaussian distribution and when not, they follow a t_ν distribution. The combination of Bayesian inference and MCMC sampling is again proven successful when estimating model parameters.

References

- [1] S. Wesolowski, I. Svensson, A. Ekström, *et al.*, “Rigorous constraints on three-nucleon forces in chiral effective field theory from fast and accurate calculations of few-body observables”, *Physical Review C*, vol. 104, no. 6, Dec. 2021, ISSN: 2469-9993. DOI: [10.1103/physrevc.104.064001](https://doi.org/10.1103/PhysRevC.104.064001). [Online]. Available: <http://dx.doi.org/10.1103/PhysRevC.104.064001>.
- [2] T. A. Lähde and U. G. Meißner., *Nuclear Lattice Effective Field Theory An Introduction*. Gewerbestrasse 11, 6330 Cham, Switzerland: Springer, 2019, ISBN: 978-3-030-14187-5.

Appendix

A Trace plots

In this appendix, trace plots for parameters c_D and c_E in all runs and Q for the extra task are provided.

Firstly, figure 1 contain traces the parameters from the run with set 1; two observables. In this case, both parameters have uncorrelated samples and there seems to be a fast convergence. From these plots, initial guesses c_D and c_E were both set to $\mathcal{N}(\mu = 0, \sigma = 1)$.

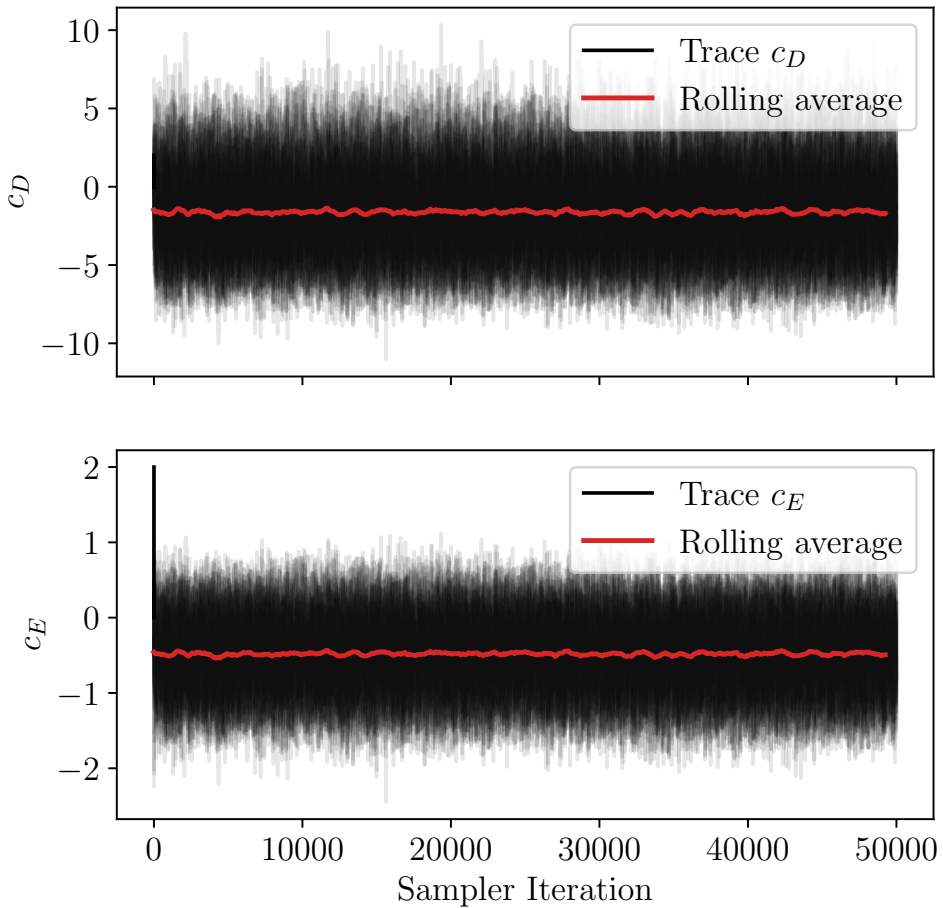


Figure 1: Trace plots for c_D and c_E with two observables.

Secondly, figure 2 contain traces of set 2; four observables. Similar to figure 1, both parameters show uncorrelated samples and a fast convergence. The first samples for c_E show slightly more deviation.

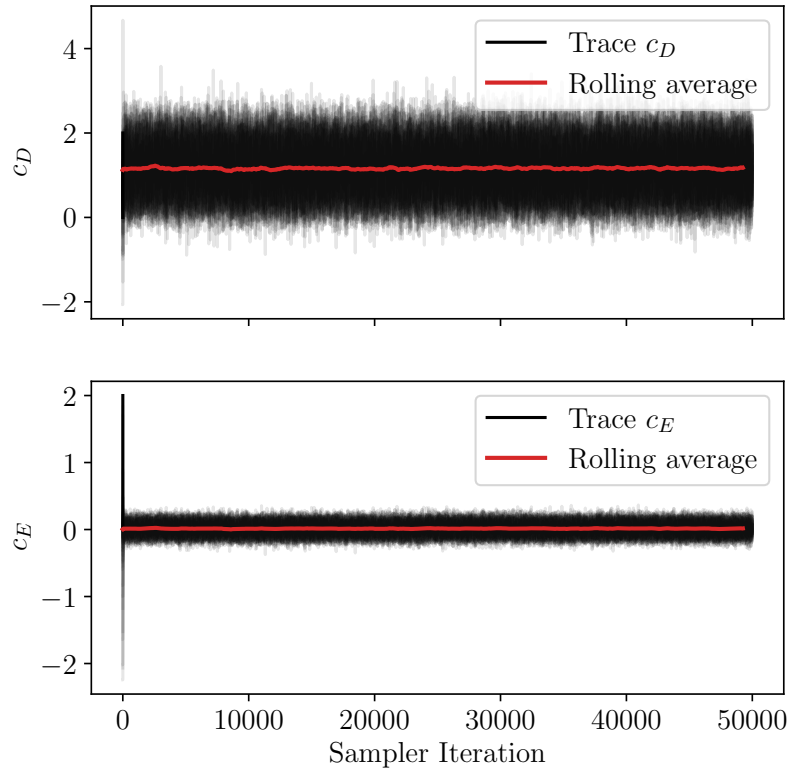


Figure 2: Trace plots for c_D and c_E with four observables.

Lastly, figure 3 contain traces of parameters and error parameter Q .

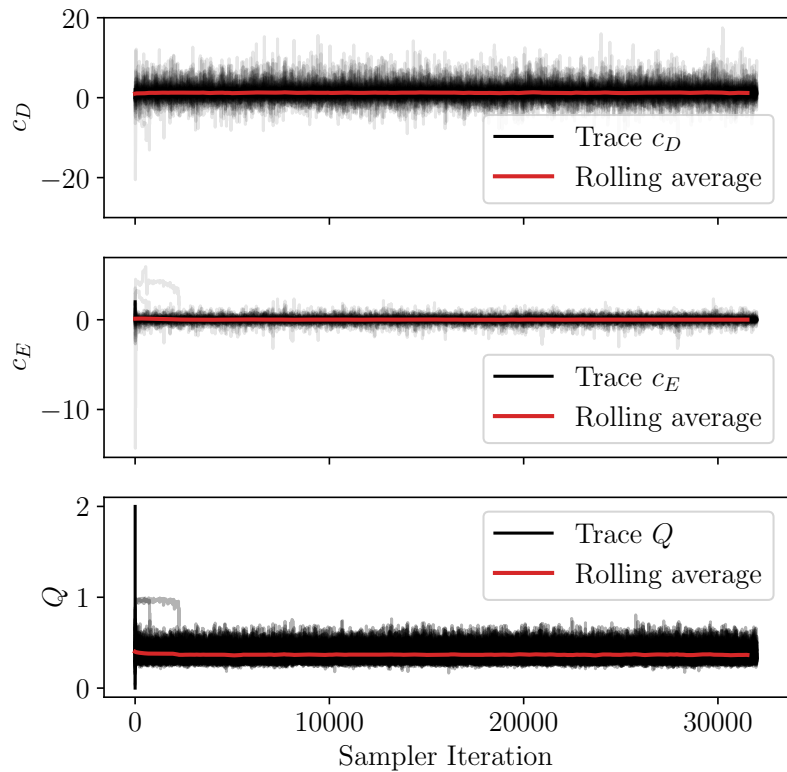


Figure 3: Trace plots for c_D , c_E and Q with four observables.

B Multivariate t -distribution fit

Here we briefly describe our method of fitting a multivariate t -distribution to the samples obtained when sampling the joint posterior with model parameters c_D and c_E , along with EFT error parameter Q . First, the individual samples of each parameter was fitted to a 1D t -distribution. From here, the degrees of freedom ν_{fit} for the multivariate fit was computed as a mean of the ν -values obtained from each 1D fit. To estimate the scale matrix S , we used the `numpy` library to compute the covariance matrix for the samples. Then, S can be obtained by the relation

$$S = \frac{\nu_{fit} - 2}{\nu_{fit}} C,$$

where C is the covariance matrix [1]. For plotting the 1D-fitted curves of the histogram, the fit parameters were used to create a 1D t -distribution PDF using `scipy`. For the contour plots, the `scipy` library was used to create a multivariate t -distribution object, which then was used to visualize the filled contours.

C Sampling the error parameter Q

The figure below shows the pure MCMC samples in a corner plot when also sampling with the error parameter Q . Note that the parameters c_D and c_E essentially are uncorrelated with Q , which is expected since they describe and enter the model in different ways. We also note that the distribution of Q differs from the Gaussian (t)-looking distributions of c_D and c_E , and that it very much resembles its prior distribution, which was a Beta distribution with parameters $a = 3$ and $b = 5$.

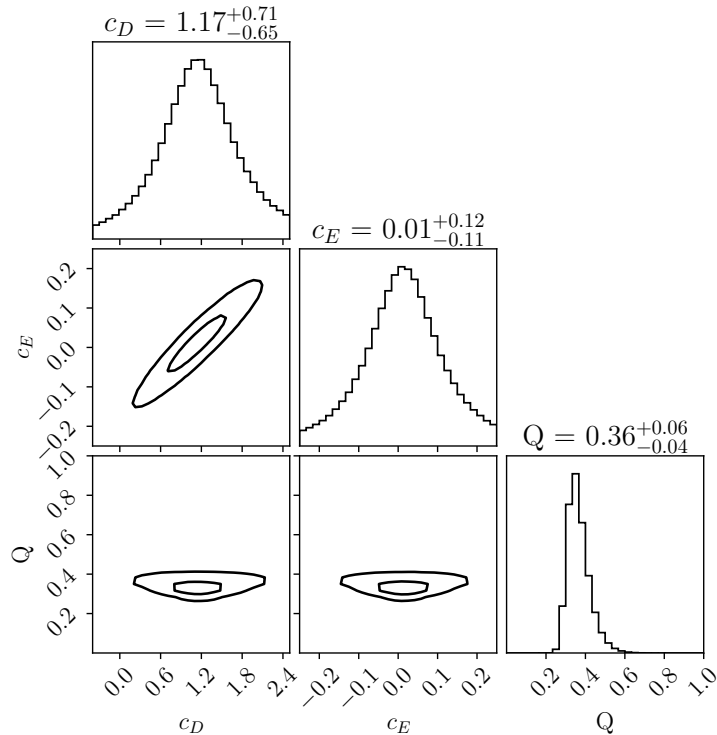


Figure 4: Corner plot after sampling with the additional parameter Q from the EFT error. The plots corresponds to the pure MCMC samples and black contours denote the 30 % and 72 % probability density mass regions, which would correspond to 1- and 2σ intervals for the fitted multivariate t -distribution for the c_D and c_E samples.